JOURNAL OF AIRCRAFT
Vol. 36, No. 4, July–August 1999

Cost-Effective Multipoint Design of a Blended High-Speed Civil Transport

Natasha E. Sevant,* Malcolm I. G. Bloor,† and Michael J. Wilson‡
University of Leeds, Leeds, England LS2 9JT, United Kingdom

The multipoint design of a high-speed civil transport (HSCT) is considered. Low computational costs are maintained by parameterizing the HSCT using a novel method of surface generation known as the partial differential equation method. This method enables a reduction in the computational costs because of its ability to describe complex surfaces using a small number of parameters. The two design points that are considered are the subsonic and supersonic (Mach 2) flight regimes with design criteria of maximized lift and minimized wave drag, respectively. Subsonic lift is estimated using Panel Method Ames Research Center, whereas supersonic wave drag is estimated using the Harris wave-drag code (which is based upon linearized potential flow theory and the supersonic area rule). An efficient quasi-Newton method of optimization is used to optimize a weighted combination of subsonic lift and supersonic wave drag subject to the constraints of a fixed wing plan area and fixed fuselage and wing volumes. A variety of test problems are considered in which the weightings of the two design criteria are varied.

Nomenclature

a, a_{f_j}, a_{w_j} = smoothing parameters
C_{D_w} = coefficient of wave drag
C_L, C_l = total and section coefficients of lift
c = reference length
c_i = aerofoil chord lengths
D_w = wave drag
$\boldsymbol{dS}_H, \boldsymbol{dS}_W$ = surface elements on high-speed civil transport (HSCT) and wake
$f(\boldsymbol{X})$ = multipoint objective function
K_P = parameter depending on position of P relative to S_H
L, L' = total lift and lift per unit span
l = length of body
n = order of Fourier mode
$\boldsymbol{n}$ = unit normal vector
$\boldsymbol{n}_f$ = vector normal to fuselage
P = point
p_1, p_2 = weighting coefficients
q_∞ = freestream dynamic pressure
r = distance between P and either $\boldsymbol{dS}_H$ or $\boldsymbol{dS}_W$
r_i = radii of fuselage cross sections
S = wing plan area, cross-sectional area, or reference area
S_H, S_W = surfaces of the HSCT and the wake
$s_{f_i}, s_{f_{ij}}, s_{f_{x_i}}, s_{f_{r_i}}$ = derivative boundary condition parameters of fuselage
$s_{w_0}, s_{w_{ij}}, s_{wx_{i0}}, s_{wx_{i1}}, s_{wy_i}$ = derivative boundary condition parameters of wing
$t_{1_i}, t_{2_i}, t_{3_i}$ = aerofoil thickness and camber parameters
u, v = parametric surface coordinates
$\boldsymbol{x}$ = Cartesian coordinates, (x, y, z)
x, x_1 = axial locations along body
$\boldsymbol{x}_f, \boldsymbol{x}_{f_u}$ = positional and derivative boundary conditions of fuselage
x_{f_i}, z_{f_i} = axial and vertical positions of fuselage boundary conditions
x_i, z_i = x and z coordinates of template aerofoil
$\boldsymbol{x}_w, \boldsymbol{x}_{w_u}$ = positional and derivative boundary conditions of wing
$\boldsymbol{x}_{w_i}$ = axial, spanwise, and vertical positions of wing boundary conditions, $(x_{w_i}, y_{w_i}, z_{w_i})$
$\boldsymbol{x}_0, \boldsymbol{x}_n^c, \boldsymbol{x}_n^s$ = functions of parametric coordinate u
α_i = angle of incidence of wing boundary conditions
θ = roll angle
μ = HSCT doublet strength distribution
μ_P = doublet strength at point P
μ_W = wake doublet strength distribution
ρ = density
σ = HSCT source strength distribution
Φ = velocity potential
Φ_P = velocity potential at point P
ϕ_∞ = onset velocity potential
ϕ_{∞_P} = onset velocity potential at point P
Ω = two-dimensional parameter domain
$\partial\Omega$ = boundary of parameter domain Ω

Introduction

OWING to recent predictions of a major increase in the world aviation market and, also, the desire for speed, there is a renewed interest in the design of high-speed civil transport (HSCT).[1] The present-day investigations are addressing many of the challenging environmental and economic issues that are associated with HSCT. In particular, the environmental problems associated with sonic boom restrict HSCT to subsonic speeds over populous land. The aerodynamic design of an HSCT needs to be considered, therefore, at both subsonic and supersonic speeds.

There are three approaches to aerodynamic design using computational fluid dynamics (CFD). The first is the traditional trial-and-error approach, where the CFD analysis code is used together with a designer's knowledge and experience in the search for better aircraft. The second approach is inverse design, which involves solving for a geometry that satisfies a prescribed distribution (usually either pressure or velocity). Finally, the third approach is direct numerical optimization, which involves coupling an aerodynamic analysis method with a scheme for numerical minimization, where the aim is the direct attainment of certain aerodynamic goals such as maximum lift and/or minimum drag.

Presented as Paper 98-2785 at the AIAA 16th Applied Aerodynamics Conference, Albuquerque, NM, 15–18 June 1998; received 27 July 1998; revision received 26 October 1998; accepted for publication 6 February 1999.

*Research Fellow, Department of Applied Mathematics. Member AIAA.
†Professor, Department of Applied Mathematics. Member AIAA.
‡Reader, Department of Applied Mathematics. Member AIAA.

The latter of these approaches, direct numerical optimization, has many advantages. It is more automatic and less influenced by designer intuition than the trial-and-error approach. It is easier to implement than the inverse design approach, and, because only solutions of the aerodynamic analysis are required, it can, in principle, use any existing CFD code. Also, whereas nothing guarantees the best solution in either the trial-and-error or the inverse design approaches, direct numerical optimization seeks optimal aircraft designs.

A further advantage of direct numerical optimization over inverse methods is that several design points can be considered simultaneously. The design point of many aircraft is the combination of the altitude and the speed (i.e., Mach number) at which the aircraft spends a considerable proportion of its flying time.[2] Although other considerations, such as takeoff and landing distances, cannot be omitted, the design of many such aircraft is often concentrated at this point. Certain aircraft, however, have two or more, perhaps conflicting, design points, for example, the subsonic and supersonic flight regimes of an HSCT. Multiple point (or multipoint) design enables a designer to find a compromise between several such conflicting requirements.[3]

Despite these advantages, direct numerical optimization has a major drawback. This is its computational expense, which arises from the numerous calls that must be made to the aerodynamic analysis methods. Naturally, the number of these calls increases with the number of parameters that are used to describe the aircraft's geometry. In fact, Labrujère and Slooff[4] remark that "In 3-D wing design especially, the number of design variables is so large that practical application of the concept seems to be remote." The simplest expedient, of course, is to reduce the number of design variables that are permitted to vary in the optimization process. However, if this reduction in the number of design variables results in a restricted range of aircraft shapes, the advantages of numerical optimization will be compromised.

This paper addresses the problem of computational expense by using a novel approach to geometry parameterization, known as the partial differential equation (PDE) method. This method is able to parameterize complex geometries both efficiently and without severely limiting the range of available shapes. It therefore both increases the feasibility and enhances the potential of direct numerical optimization of aircraft geometries.

In the following sections, the PDE method is described and then applied to the generation of an HSCT. Also described are the aerodynamic analysis methods and the methods of optimization and constraint satisfaction. The multipoint design of an HSCT with fuselage volume and wing plan area and volume constraints is then considered. The composite design criterion incorporates both subsonic lift and supersonic wave drag. Weighted coefficients are used to alter the balance between these two design criteria in order to optimize aircraft for various types of design missions. For instance, because an HSCT will typically perform the majority of its range at supersonic speeds, more emphasis should be placed upon the minimization of supersonic wave drag. (On the other hand, interceptor aircraft may perform most of their range at subsonic speeds with occasional spurts at supersonic speeds.)

Without the incorporation of all factors affecting the performance and, indeed, the construction of an aircraft, the design of a completely plausible configuration is unlikely. It is therefore necessary to clarify the purposes of this paper as demonstrating both the efficiency and the capabilities of the PDE method, rather than as the design of completely realistic HSCT.

PDE Method

The PDE method is an innovative method of surface generation, which was devised by Bloor and Wilson.[5] It was applied, originally, to the generation of blending surfaces and, subsequently, to the generation of free-form surfaces.[6] The versatility of the PDE method has been demonstrated by producing various surfaces of practical significance, such as generic aircraft geometries[7,8] and marine propellers.[9] The PDE method has also been implemented in the functional design of, for example, a yacht hull, a swirl port, and a subsonic wing-body combination.[10]

In the PDE method a surface is regarded as the solution of a boundary-value problem in which a parametric function $\boldsymbol{x}(u, v)$, defined over a domain Ω in two-dimensional (u, v) parameter space, is sought that satisfies specified boundary conditions around the edge $\partial\Omega$ of that domain. The Euclidean coordinates of points on the surface are given by the function $\boldsymbol{x}(u, v) = [x(u, v), y(u, v), z(u, v)]$ while the parametric coordinates u and v define a curvilinear coordinate system on the surface. To obtain the function $\boldsymbol{x}$, it is assumed to satisfy a suitably chosen elliptic PDE, which is then solved subject to the specified boundary conditions. Typically, these boundary conditions will be in the form of $\boldsymbol{x}$ and a number of its derivatives. The number and order of the specified derivatives are determined by the required degree of continuity between the surface and any adjacent patches and/or the required control of the shape of the surface.

Much of the previous work has been based upon the following fourth-order elliptic PDE:

$$\left(\frac{\partial^2}{\partial u^2} + a^2\frac{\partial^2}{\partial v^2}\right)^2 \boldsymbol{x} = 0 \tag{1}$$

where a is known as the smoothing parameter and the boundary conditions usually specify the variance of $\boldsymbol{x}$ and its normal derivative $\partial\boldsymbol{x}/\partial n$ along $\partial\Omega$. The boundary conditions on $\boldsymbol{x}$ specify both the shape and the position or, more specifically, the parameterization of the boundaries of the surface in physical space, whereas the boundary conditions on the normal derivative of $\boldsymbol{x}$ control the direction and speed of departure of the surface from its boundaries. The smoothing parameter a controls the relative scaling between the u and v parametric directions and thus provides an additional dimension to the control of the surface's shape. Equation (1) represents a smoothing process between the conditions on the boundaries of the surface patch where, in some sense, the value of the function at any point on the surface is a weighted average of the surrounding values.

Many surfaces can be represented by a looped surface patch bounded by two closed curves or can be constructed from a collection of such patches. For surfaces such as these, it is convenient to take the coordinate domain Ω to be a rectangle where one of the surface coordinates, e.g., u, varies as the surface sweeps from one boundary curve to the other, while the other surface coordinate v varies around the patch. Choosing the v interval to be $[0, 2\pi]$ yields a parametric function $\boldsymbol{x}(u, v)$ with a period of 2π in v, which can thus be expressed in terms of a Fourier series expansion, as follows:

$$\boldsymbol{x}(u, v) = \boldsymbol{x}_0(u) + \sum_{n=1}^{\infty} \boldsymbol{x}_n^c(u)\cos nv + \sum_{n=1}^{\infty} \boldsymbol{x}_n^s(u)\sin nv \tag{2}$$

where the components of the vectors $\boldsymbol{x}_0$, $\boldsymbol{x}_n^c$, and $\boldsymbol{x}_n^s$ are functions of u. Substituting this Fourier series expansion into Eq. (1) yields a series of uncoupled and identical linear homogeneous ordinary differential equations (ODE) for the functions $\boldsymbol{x}_0$, $\boldsymbol{x}_n^c(u)$, and $\boldsymbol{x}_n^s(u)$; each of which have a solution that is dependent upon the relevant Fourier mode of the boundary conditions. If a particular Fourier mode is absent from all of the boundary conditions imposed on $\boldsymbol{x}$, the solution of the ODE corresponding to that mode will be zero. Therefore, when the boundary conditions are either given or can be expressed as finite Fourier series, the series solution given by Eq. (2) is also finite and contains only those Fourier modes that are present in the boundary conditions.

In the case of more general boundary conditions, which cannot be expressed as finite Fourier series, Bloor and Wilson have developed a rapid approximate method of solution.[11] This method involves approximating the boundary conditions using finite Fourier series [$n \geq 5$ in Eq. (2), say] and then adding a remainder term, which accounts for the discrepancy between the original and the approximate boundary conditions.

HSCT Geometry

The HSCT considered in this paper is composed of a fuselage, a fuselage-wing fairing (or blend), an inner wing and an outer wing,

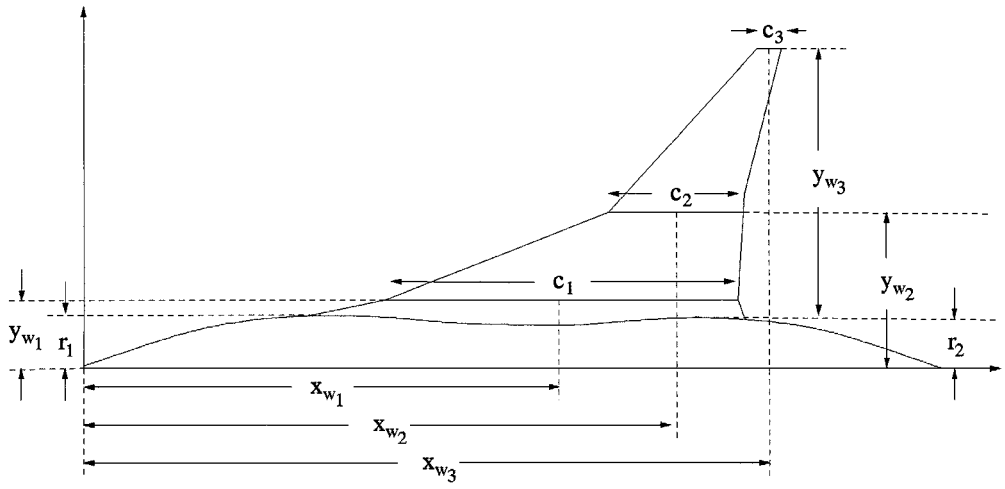

Fig. 1 HSCT design parameters.

as illustrated in Fig. 1. All of these four components are generated using the PDE method.

The fuselage is divided into three PDE surface patches that define forward, middle, and rearward components. PDE boundary conditions are thus required at the fuselage's nose ($u = 0$), at two intermediate stations ($u = 1$ and $u = 2$), and the base ($u = 3$). The fuselage's nose and base are assumed to be smooth and rounded, whereas the cross sections at the intermediate sections are assumed to be circular.

The general form of the positional and derivative boundary conditions at the nose and base of the fuselage are taken to be

$$\boldsymbol{x}_f(i, v) = \left(x_{f_i}, 0, z_{f_i}\right), \qquad \boldsymbol{x}_{f_u}(i, v) = s_{f_i}(0, \cos v, \sin v) \tag{3}$$

whereas those at the intermediate stations are taken to be

$$\begin{aligned} \boldsymbol{x}_f(i, v) &= \left(x_{f_i}, r_i \cos v, z_{f_i} + r_i \sin v\right) \\ \boldsymbol{x}_{f_u}(i, v) &= \left(s_{f_{x_i}}, s_{f_{r_i}} \cos v, s_{f_{r_i}} \sin v\right) \end{aligned} \tag{4}$$

where v varies in the range $0 \le v \le 2\pi$ and $i = 0$, 1, 2, and 3 at the nose, the intermediate stations and the base, respectively. The parameters x_{f_i} and z_{f_i} define the axial and vertical positions of each of these boundary conditions (x_{f_0} and z_{f_0} are taken to be zero such that the nose lies at the origin of the Cartesian coordinate system). At the intermediate stations the parameters r_i define the radii of the circular cross sections (see Fig. 1). The direction and magnitude of the derivative boundary conditions at the fuselage's nose and base are controlled by the parameters s_{f_i}, whereas those at the intermediate stations are controlled by the parameters $s_{f_{x_i}}$ and $s_{f_{r_i}}$. When solving for the forward, middle, and rearward components, the derivative boundary conditions at the intermediate stations are multiplied by scaling factors $s_{f_{ij}}$, which act upon the ith boundary condition of the jth fuselage component, and the smoothing parameter of each component is defined to be a_{f_j} ($j = 1$, 2, and 3 corresponding to the forward, middle, and rearward components, respectively).

The entire wing is also generated from three PDE surface patches, which form the fuselage-wing fairing, the inner wing, and the outer wing. Each of these PDE surface patches are bounded by aerofoil-type closed curves; the first aerofoil curve ($u = 0$) lies on the surface of the fuselage, whereas the second ($u = 1$), third ($u = 2$), and fourth ($u = 3$) form the root, crank, and tip aerofoil sections of the wing. A simple template cambered aerofoil, of unit chord length, is given by the following Fourier series expansion:

$$x_i(v) = \tfrac{1}{2}\cos v, \qquad z_i(v) = t_{1_i} \sin v + t_{2_i} \sin 2v + \tfrac{1}{2} t_{3_i}(1 - \cos 2v) \tag{5}$$

where v varies in the range $0 \le v \le 2\pi$ and the Fourier coefficients t_{1_i} and t_{2_i} define the thickness distribution of the aerofoil while t_{3_i} controls the camber.

The aerofoil boundary curve upon the surface of the fuselage is given by

$$\boldsymbol{x}_w(0, v) = \begin{bmatrix} x_{w_0} + c_0(x_1 \cos\alpha_0 + z_1 \sin\alpha_0) \\ y_f(u_f, v_f) \\ z_{w_0} + c_0(z_1 \cos\alpha_0 - x_1 \sin\alpha_0) \end{bmatrix} \tag{6}$$

where x_{w0} and z_{w0} are the axial and vertical positions of the midchord point of the aerofoil and the parameters c_0 and α_0 are the chord length and angle of incidence of the aerofoil. The y coordinates of this boundary condition are obtained by solving numerically for the values u_f and v_f of u and v on the surface of the fuselage $\boldsymbol{x}_f$ that satisfy the x and z coordinates of Eq. (6). A localized annular region on the surface of the fuselage, bounded by Eq. (6) and an enclosing rectangular box specified in (u, v) space, is then reparameterized in order to accommodate the aerofoil hole.

The derivative boundary conditions at $u = 0$ are such that the fairing is tangent plane continuous with the fuselage. These are defined as

$$\boldsymbol{x}_{w_u}(0, v) = s_{w0} \hat{\boldsymbol{x}}_{w_u}(0, v) \sin v \tag{7}$$

where

$$\hat{\boldsymbol{x}}_{w_u}(0, v) = \frac{\boldsymbol{n}_f(u_f, v_f) \times \boldsymbol{x}_{w_v}(0, v)}{\left|\boldsymbol{n}_f(u_f, v_f) \times \boldsymbol{x}_{w_v}(0, v)\right|} \tag{8}$$

and $\boldsymbol{n}_f(u_f, v_f)$ is the normal to the fuselage and $\boldsymbol{x}_{w_v}(0, v)$ is the derivative of the boundary curve given by Eq. (6) with respect to v. The scaling term $s_{w_0} \sin v$, in Eq. (7), varies the magnitude of the derivative boundary condition around the aerofoil section such that it is reduced as the aerofoil tapers toward its trailing edge.

The general positional boundary conditions at the wing root ($i = 1$), crank ($i = 2$), and tip ($i = 3$) are taken to be

$$\boldsymbol{x}_w(i, v) = \boldsymbol{x}_{w_i} + c_i \begin{pmatrix} x_1 \cos\alpha_i + z_1 \sin\alpha_i \\ 0 \\ z_1 \cos\alpha_i - x_1 \sin\alpha_i \end{pmatrix} \tag{9}$$

where $\boldsymbol{x}_{w_i} = (x_{w_i}, y_{w_i}, z_{w_i})$ are the axial, spanwise (see Fig. 1), and vertical positions of the midchord points of the root, crank, and tip aerofoils, and the parameters c_i and α_i define the chord lengths and the angles of incidence of these aerofoil sections.

Table 1 Parameter values of the baseline HSCT

Fuselage parameters					
x_{f_0}	=	0.0	z_{f_0}	=	0.0
x_{f_1}	=	20.0	z_{f_1}	=	0.0
x_{f_2}	=	85.0	z_{f_2}	=	0.0
x_{f_3}	=	100.0	z_{f_3}	=	0.0
r_1	=	2.7	r_2	=	2.6
s_{f_0}	=	1.0	$s_{f_{22}}$	=	1.0
$s_{f_{11}}$	=	1.0	$s_{f_{23}}$	=	0.3
$s_{f_{12}}$	=	1.0	s_{f_3}	=	1.0
$s_{f_{x_1}}$	=	40.0	$s_{f_{x_2}}$	=	30.0
$s_{f_{r_0}}$	=	2.0	$s_{f_{r_1}}$	=	1.0
$s_{f_{r_2}}$	=	−1.0	$s_{f_{r_3}}$	=	−2.0
a_{f_1}	=	2.0	a_{f_2}	=	3.5
a_{f_3}	=	1.0			
Fairing and wing parameters					
x_{w_0}	=	53.5	x_{w_1}	=	55.0
x_{w_2}	=	69.0	x_{w_3}	=	80.0
			y_{w_1}	=	3.0
y_{w_2}	=	15.0	y_{w_3}	=	25.0
z_{w_0}	=	−0.2	z_{w_1}	=	−0.2
z_{w_2}	=	−0.2	z_{w_3}	=	−0.2
c_0	=	50.0	c_1	=	43.0
c_2	=	15.0	c_3	=	3.0
t_{1_0}	=	0.025	t_{1_1}	=	0.02
t_{1_2}	=	0.02	t_{1_3}	=	0.02
t_{2_0}	=	−0.003	t_{2_1}	=	−0.004
t_{2_2}	=	−0.004	t_{2_3}	=	−0.004
t_{3_0}	=	0.002	t_{3_1}	=	0.003
t_{3_2}	=	0.003	t_{3_3}	=	0.0
α_0	=	1.0	α_1	=	1.0
α_2	=	1.0	α_3	=	0.0
s_{w_0}	=	1.0			
$s_{w_{10}}$	=	1.0	$s_{w_{11}}$	=	1.0
$s_{w_{21}}$	=	1.0	$s_{w_{22}}$	=	1.0
$s_{wx_{10}}$	=	0.0	$s_{wx_{11}}$	=	2.0
$s_{wx_{20}}$	=	5.0	$s_{wx_{21}}$	=	4.0
$s_{wx_{30}}$	=	1.0	$s_{wx_{31}}$		0.0
s_{wy_1}	=	1.0	a_{w_1}	=	1.0
s_{wy_2}	=	5.0	a_{w_2}	=	1.0
s_{wy_3}	=	1.0	a_{w_3}	=	1.0

Finally, the general derivative boundary conditions at the wing root, crank, and tip are defined to be

$$\boldsymbol{x}_{w_u}(i, v) = \begin{pmatrix} s_{wx_{i0}} - s_{wx_{i1}} \cos v \\ s_{wy_i} \\ 0 \end{pmatrix} \tag{10}$$

where the direction of the localized wing sweep at these sections is controlled by the parameters $s_{wx_{i0}}$, $s_{wx_{i1}}$, and s_{wy_i}. When solving for the fairing and the inner and outer wings, the derivative boundary conditions at the wing root and crank are multiplied by scaling factors $s_{w_{ij}}$, which act upon the ith derivative boundary condition of the jth wing component and the smoothing parameter of each component is defined to be a_{w_j} ($j = 1, 2, 3$ corresponding to the fairing and the inner and outer wings, respectively).

The boundary conditions of the three fuselage surface patches and the inner and outer wings are such that the PDE given by Eq. (1) can be solved using the exact Fourier series solution, as described in the preceding section, whereas the fuselage-wing fairing is solved for using the approximate method described in Ref. 11.

A baseline HSCT is illustrated in Fig. 2, and the corresponding parameter values are given in Table 1.

Aerodynamic Analyses

Subsonic Lift

A low-order potential flow panel method, known as PMARC,[12] is used to estimate the lift of the HSCT. Panel methods are based on the assumption that, for high Reynolds number and attached flow conditions, the regions of the flowfield dominated by viscous and rotational effects are confined to thin boundary layers and wakes.

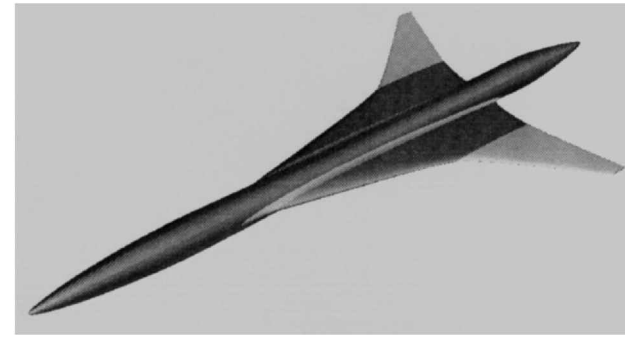

Fig. 2 Baseline HSCT design.

The remainder of the flowfield is assumed to be inviscid, irrotational, and also incompressible. Thus, a velocity potential Φ can be defined, and the incompressible continuity equation reduces to Laplace's equation: $\nabla^2 \Phi = 0$.

The solution of Laplace's equation yields an integral equation for the velocity potential Φ_P at any point P expressed in terms of an unknown distribution of sources σ and doublets μ across the surface of the HSCT S_H and an unknown distribution of doublets μ_W across the surface of its wake S_W:

$$\Phi_P = \frac{1}{4\pi} \iint_{S_H - P} \mu \, \boldsymbol{n} \cdot \nabla\left(\frac{1}{r}\right) dS_H + \frac{1}{4\pi} \iint_{S_H} \left(\frac{\sigma}{r}\right) dS_H + \frac{1}{4\pi} \iint_{S_W} \mu_W \, \boldsymbol{n} \cdot \nabla\left(\frac{1}{r}\right) dS_W + \frac{1}{4\pi} K_P \mu_P + \phi_{\infty_P} \tag{11}$$

where r is the distance from the surface elements dS_H and dS_W to the point P, $\boldsymbol{n}$ is the unit normal vector that points into the flowfield of interest, μ_P is the doublet value at the point P, ϕ_{∞_P} is the onset velocity potential at the point P the subscript $S_H - P$ signifies that the point P is excluded from the first surface integral, and the value of the parameter K_P depends on where P lies with respect to the surface of the HSCT.[12]

Equation (11) must satisfy the Neumann boundary condition, which states that the velocity component normal to the surface of the HSCT S_H is zero. Also, because potential flow is irrotational, a physically-based condition must be introduced to fix the amount of circulation and, equivalently, the amount of lift generated by the HSCT's wing. In PMARC the amount of lift generated by a wing is fixed using the Kutta condition, which states that the velocity at the wing's trailing edge is finite.

Even subject to the Neumann boundary and Kutta conditions, an infinite number of source and doublet distributions will satisfy Laplace's equation, each of which yields the same external flowfield but different fictitious flowfields within the interior of the HSCT. To obtain a unique solution, PMARC sets the fictitious internal velocity potential equal to the onset velocity potential ϕ_∞—a condition which is known as the internal Dirichlet boundary condition. The doublet distribution μ then becomes the perturbation potential caused by the HSCT and the source distribution σ, which is the jump in the normal velocity component on the surface of the HSCT S_H, and can thus be determined using the external Neumann and internal Dirichlet boundary conditions. Substituting this source distribution into Eq. (11) when the point P lies on the inner surface of the HSCT yields an integral equation to be solved for the unknown doublet distribution μ.

To obtain the unknown doublet distribution, the surfaces of the HSCT and its wake are discretized into a number of quadrilateral panels, upon each of which (because PMARC is a low-order panel method) constant source and doublet strengths are assumed. The PDE-generated HSCT considered herein is easily discretized by subdividing the (u, v) coordinate domain.

The internal Dirichlet boundary condition is satisfied at control points placed at the center of each of the HSCT's surface panels. This yields a set of linear simultaneous equations that can be solved for the unknown HSCT doublet strengths. The wake doublet strengths

are determined using the Kutta condition, which implies that the circulation at the wing's trailing edge must be zero and therefore that the doublet strengths of the first row of wake panels should cancel the combined doublet strengths of the two rows of panels that form the trailing edge of the wing. Although PMARC has the capability to time-step wakes, in the present application computational expense is reduced by shedding the wake doublet strengths down each streamwise column on a prescribed wake surface.

Substituting the doublet and source strengths back into the discretized form of Eq. (11) yields the velocity potential at the control point of each of the HSCT's panels. The velocity components are then given by the gradient of the velocity potential from which the resultant speeds can be calculated. For steady flow the pressure coefficients of each panel can then be calculated using Bernoulli's equation.

With the pressure distribution over the surface of the HSCT known, the resultant force contributions from each panel can be evaluated. These force contributions can be summed up panel by panel to give the resultant aerodynamic force on the body. The lift L is the component of this resultant force perpendicular to the freestream direction, and the section and total lift coefficients C_l and C_L are defined by

$$C_l \equiv L'/q_\infty c, \qquad C_L \equiv L/q_\infty S \tag{12}$$

where q_∞ is the freestream dynamic pressure, c is a reference length (usually chosen to be the chord length of the aerofoil section), S is a reference area (usually chosen to be the plan area of the wing), and the prime of L' denotes the lift force per unit span.

Supersonic Wave Drag

Wave drag, which is caused by the energy radiated away from an aircraft in the form of pressure or shock waves,[13] is estimated using the classic Harris wave-drag program.[14] This program was developed by Boeing for NASA during the U.S. Supersonic Transport (SST) Program and is based upon linearized potential flow theory and the supersonic area rule.

Under the assumptions of linearized potential flow theory, the wave drag of a slender body of revolution in symmetric supersonic flow can be estimated by considering a distribution of sources along its axis,[15] where the strength of this lineal source distribution is proportional to the rate of change of the cross-sectional area of the body in the freestream direction. By integrating the flux of momentum across a cylindrical surface enclosing the body, von Kármán[15] showed that the wave drag D_w of a slender body of revolution, of length l and cross-sectional area $S(x)$, could be estimated by

$$\frac{D_w}{q_\infty} = -\frac{1}{\pi}\int_0^l S''(x)\,\mathrm{d}x \int_0^x S''(x_1)\ln(x - x_1)\,\mathrm{d}x_1 \tag{13}$$

where x and x_1 are axial locations along the axis of the body, the term $S''(x)$ is the second derivative of the body's cross-sectional area with respect to x, and q_∞ is the freestream dynamic pressure.

The supersonic area rule was presented by both Jones[16] and Whitcomb and Sevier.[17] It is based upon Hayes' method,[18] which states that the momentum flux along a line that is parallel to and at an infinite distance from the axis of some arbitrary source distribution, is identical to that which would result if each source were moved along the Mach plane, within which it lies, to the axis of the source distribution. If this source distribution represents the flowfield around an aircraft with a slender fuselage and thin nonlifting wings (lift-dependent wave drag is relatively small and is usually neglected in aircraft design[19]), it can be shown that the strength of the equivalent lineal source distribution is proportional to the gradient of the normal projections of the aircraft areas intercepted by a series of parallel Mach planes; i.e., the lineal source distribution represents the flowfield around a body of revolution with cross-sectional areas equal to the normal projections of those aircraft areas intercepted by the series of Mach planes. The wave drag of an equivalent body of revolution can then be estimated using von Kármán's slender body formula [Eq. (13)]. However, because the line at infinity can be placed at any azimuthal or roll angle θ around the axis of the aircraft (with each roll angle yielding a different equivalent body of revolution), the wave drag D_w of the entire configuration is taken to be the integrated average of the equivalent body wave drags obtained through a complete rotation of the roll angle θ:

$$\frac{D_w}{q_\infty} = \frac{1}{2\pi}\int_0^{2\pi} \frac{D_w(\theta)}{q}\,\mathrm{d}\theta \tag{14}$$

The problem of minimizing supersonic wave drag thus reduces to seeking an aircraft for which each equivalent body of revolution has minimum wave drag. One such body of revolution that is pointed at both ends and has minimum wave drag for given length and volume is the Sears–Haack body.[20,21] This body has a symmetrical bell-shaped cross-sectional area distribution and provides a useful guide for assessing possible reductions in wave drag.

Optimization and Constraints

Quasi-Newton Optimization

The method of numerical minimization used in this paper is a quasi-Newton method, which is known as the Broyden–Fletcher–Goldfarb–Shanno (BFGS) method.[22] Such methods use gradient information to search in descent directions for the minimum of an objective function. The direction of each such line search is determined by minimizing the second-order Taylor series expansion of the objective function. This involves evaluating or approximating both the gradient vector and the inverse Hessian matrix of the objective function. Quasi-Newton methods build up an approximation to the inverse Hessian matrix, the various different methods correspond to different ways of approximating this matrix. For simplicity, the gradient vector is approximated using finite differences. However, a more efficient way to calculate the gradient vector would be to use the Automatic Differentiation In Fortran (ADIFOR) system,[23] which automatically differentiates Fortran programs.

The BFGS quasi-Newton method is a local method of optimization; therefore, the search for a global minimum using this method involves an heuristic approach in which various alternative designs must be used to initiate the optimization process. If the optimizer converges repeatedly to either a single optimal design or a small number of optimal designs, a success in the attainment of the global optimum can be assured with reasonable confidence. However, if the optimizer persists in converging to different final designs, there is little guarantee of attaining the global minimum without performing an almost exhaustive search.

Constraint Satisfaction

There are two types of constraints in the present design problem: parameter bound constraints and nonlinear equality constraints. The first of these, parameter bound constraints, constrain a parameter between minimum and maximum values. Such constraints are satisfied using the active set method,[24] which involves monitoring each line search to check for constraint violations. If a constraint is violated, the line search is backtracked such that this constraint becomes active (i.e., satisfied as an equality). The parameter corresponding to this active constraint is then set equal to the bound value and removed from the optimization process. Once the optimizer has converged, the validity of any active constraints must be verified. If any are inactive (i.e., if a feasible perturbation from the constraint yields a reduction in the objective function), the corresponding parameter must be returned and the optimizer restarted. This process continues until all active constraints are valid.

The nonlinear equality constraints (i.e., the fuselage volume and the wing plan area and volume constraints) are satisfied by the elimination of design variables. This involves solving for the value of the eliminated parameters that satisfy these constraints exactly.

Results

In this section, a total of four HSCT design problems are considered. The multipoint objective function $f(\boldsymbol{X})$ is defined as a

Table 2a Final parameter values and coefficients of lift and wave drag of the multipoint HSCT design problems

Design variable	$(p_1 = 1.0;\ p_2 = 0.0)$	$(p_1 = 0.2;\ p_2 = 0.8)$
r_1	2.683	2.463
r_2	2.625	2.457
s_{fr_1}	0.992	1.131
s_{fr_2}	−1.099	−1.045
s_{f12}	0.970	1.009
s_{f22}	0.954	1.002
a_{f_2}	3.504	2.563
c_1	43.378	49.870
s_{w12}	1.286	0.970
a_{w_1}	0.886	0.999
x_{w_2}	62.644	73.656
y_{w_2}	5.016	7.878
c_2	26.963	16.828
s_{wx20}	4.932	5.032
s_{wx21}	6.305	3.894
s_{w23}	2.902	0.868
x_{w_3}	66.080	81.564
c_3	2.500	4.000
s_{wx30}	0.997	0.985
a_{w_2}	0.886	0.999
a_{w_3}	0.758	1.005
C_L	8.555e−2	5.721e−2
C_{D_w}	(1.588e−2)	8.802e−3

Table 2b Final parameter values and coefficients of lift and wave drag of the multipoint HSCT design problems

Design variable	$(p_1 = 0.1;\ p_2 = 0.9)$	$(p_1 = 0.0;\ p_2 = 1.0)$
r_1	2.485	2.357
r_2	2.345	2.188
s_{fr_1}	1.969	2.233
s_{fr_2}	−1.462	−1.533
s_{f12}	1.078	1.134
s_{f22}	1.007	0.976
a_{f_2}	2.726	1.895
x_{w_1}	49.756	47.702
c_1	40.825	40.520
s_{w12}	0.589	0.558
x_{w_2}	69.217	86.802
y_{w_2}	12.606	12.906
c_2	10.588	10.151
s_{wx20}	5.036	4.960
s_{wx21}	3.692	3.935
s_{w23}	0.062	0.500
x_{w_3}	73.587	79.049
c_3	3.239	3.245
s_{wx30}	1.059	1.071
a_{w_2}	0.982	0.976
a_{w_3}	1.028	1.054
C_L	5.557e−2	(3.680e−2)
C_{D_w}	6.398e−3	4.652e−3

composite function of the coefficient of subsonic lift C_L and the coefficient of supersonic wave drag C_{D_w}, as follows:

$$f(\boldsymbol{X}) = -p_1\left(C_L \big/ C_{L_0}\right) + p_2\left(C_{D_w} \big/ C_{D_{w_0}}\right) \tag{15}$$

where $\boldsymbol{X}$ is the vector of HSCT design variables that are allowed to vary in the optimization process and C_{L_0} and $C_{D_{w_0}}$ are the coefficients of subsonic lift and supersonic wave drag of the baseline HSCT. The weighting coefficients p_1 and p_2 are varied in order to alter the balance between the subsonic and supersonic design points.

A total of 21 design variables (as given in the far left column of Tables 2a and 2b) are permitted to vary in the optimization process. Of these parameters the smoothing parameter of the middle fuselage component a_{f_2} is used to satisfy the fuselage volume constraint, and the chord length c_2 and spanwise position y_{w_2} of the crank aerofoil are used to satisfy the wing plan area and volume constraints. In addition, to maintain a reasonable fuselage-wing fairing, the parameters x_{w_0} and c_0 vary such that $x_{w_0} = x_{w_1} - 1.5$ and $c_0 = c_1 + 7.0$.

The design problems considered correspond to the following combinations of p_1 and p_2: (1.0, 0.0), (0.2, 0.8), (0.1, 0.9), and (0.0, 1.0). Note that the first and last of these are in fact the subsonic lift and supersonic wave-drag single point design problems. Because the employed method of optimization optimizes only locally, various initial designs were used to initiate all of these design

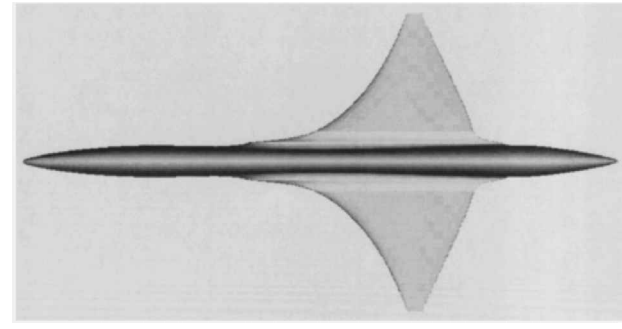

Fig. 3a Final HSCT configuration of the $(p_1 = 1.0;\ p_2 = 0.0)$ design problem.

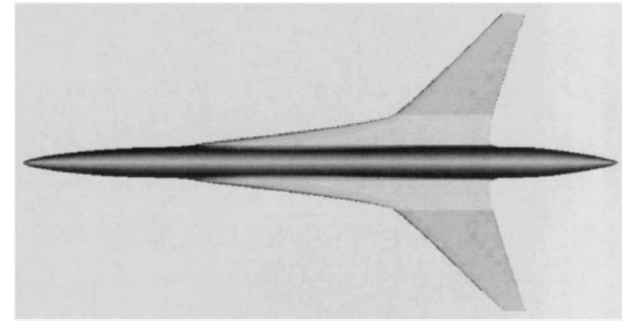

Fig. 3b Final HSCT configuration of the $(p_1 = 0.2;\ p_2 = 0.8)$ design problem.

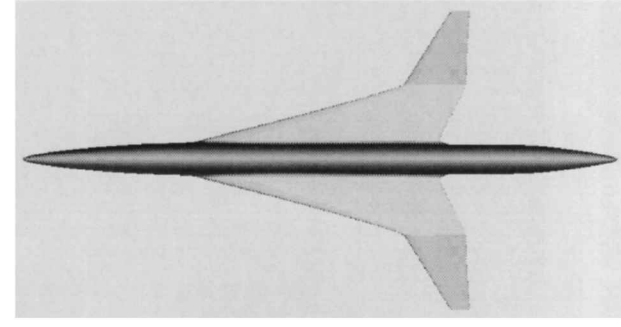

Fig. 3c Final HSCT configuration of the $(p_1 = 0.1;\ p_2 = 0.9)$ design problem.

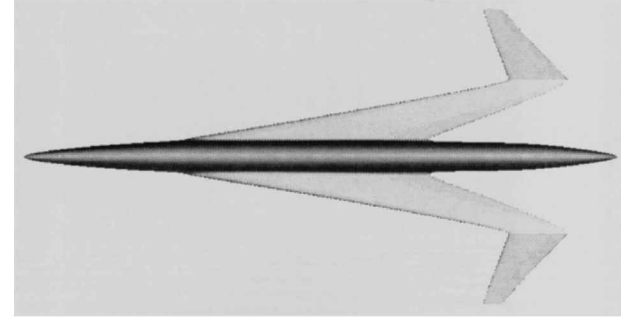

Fig. 3d Final HSCT configuration of the $(p_1 = 0.0;\ p_2 = 1.0)$ design problem.

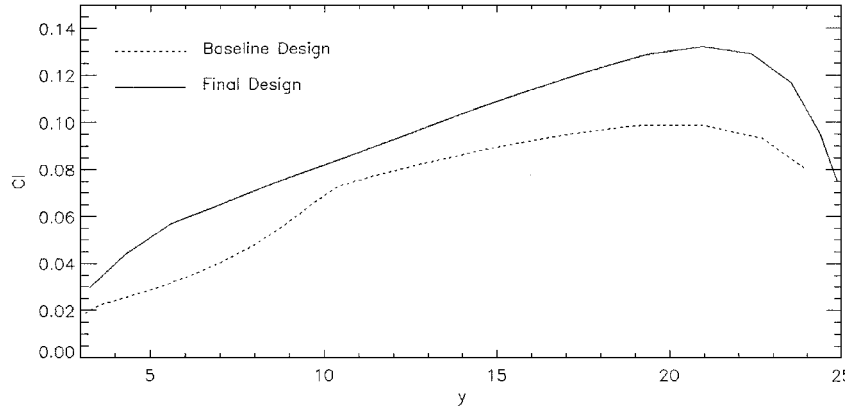

a) ($p_1 = 1.0; p_2 = 0.0$) design problem

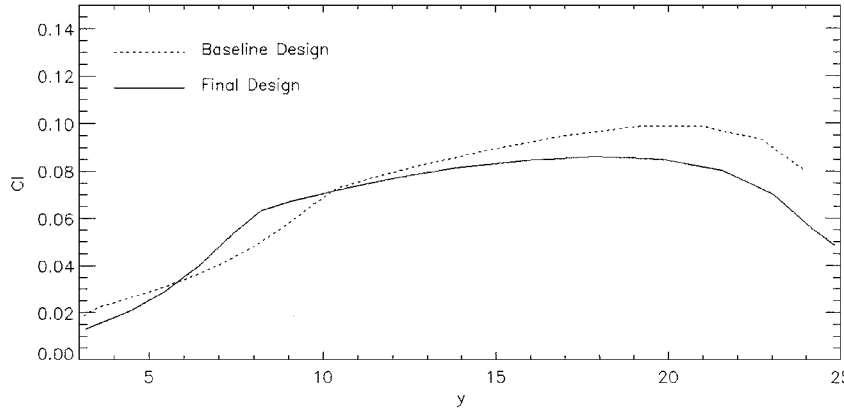

b) ($p_1 = 0.2; p_2 = 0.8$) design problem

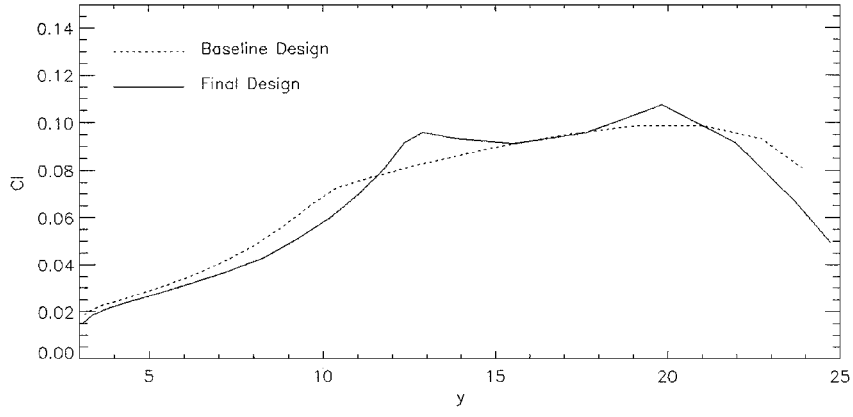

c) ($p_1 = 0.1; p_2 = 0.9$) design problem

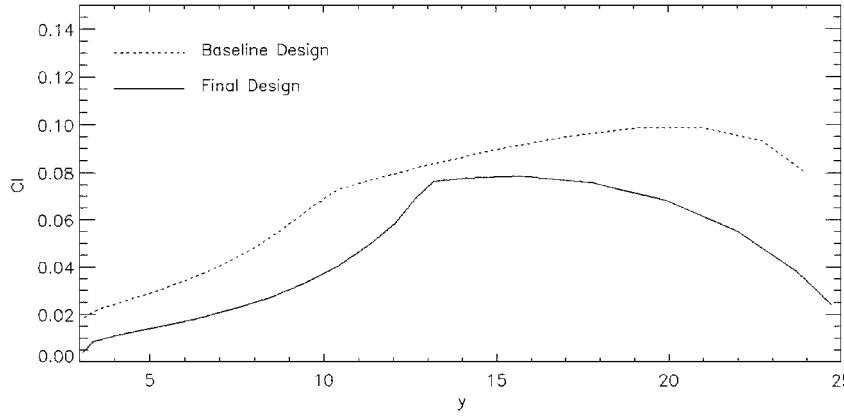

d) ($p_1 = 0.0; p_2 = 1.0$) design problem

Fig. 4 Spanwise variations of the section coefficients of lift of the baseline and HSCT designs.

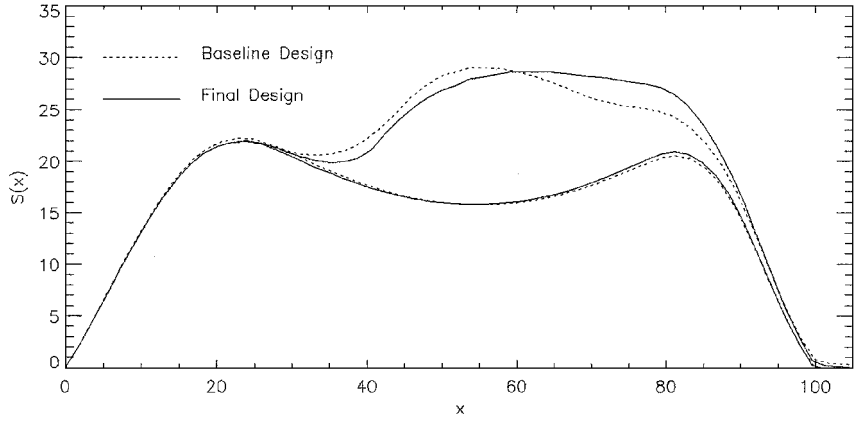

a) ($p_1 = 1.0; p_2 = 0.0$) design problem

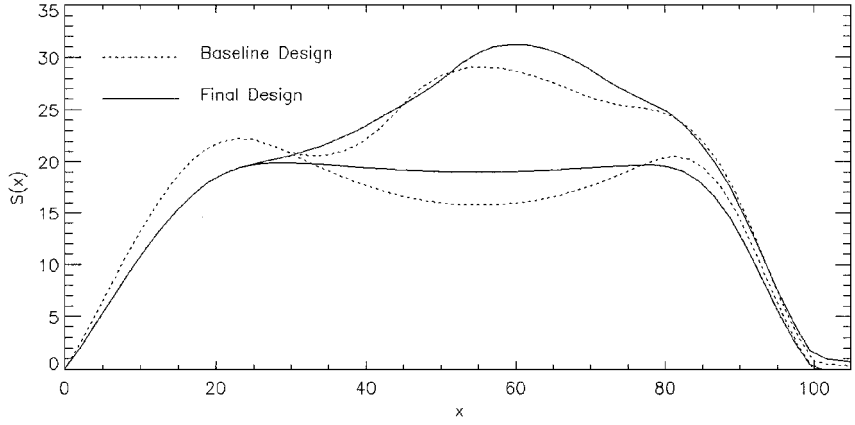

b) ($p_1 = 0.2; p_2 = 0.8$) design problem

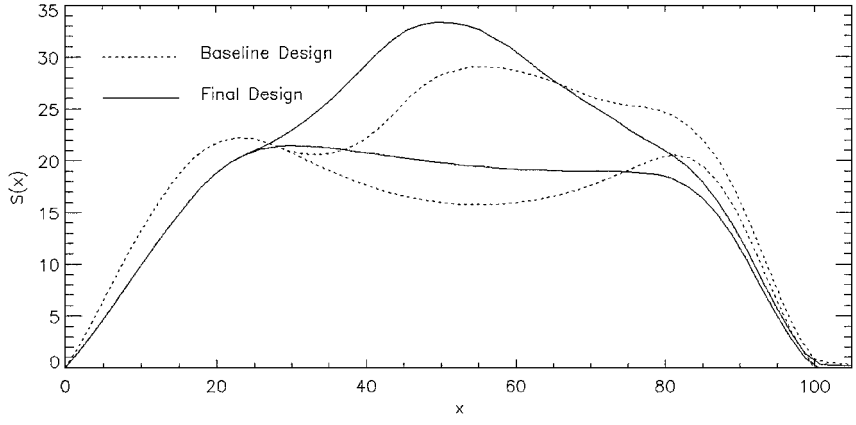

c) ($p_1 = 0.1; p_2 = 0.9$) design problem

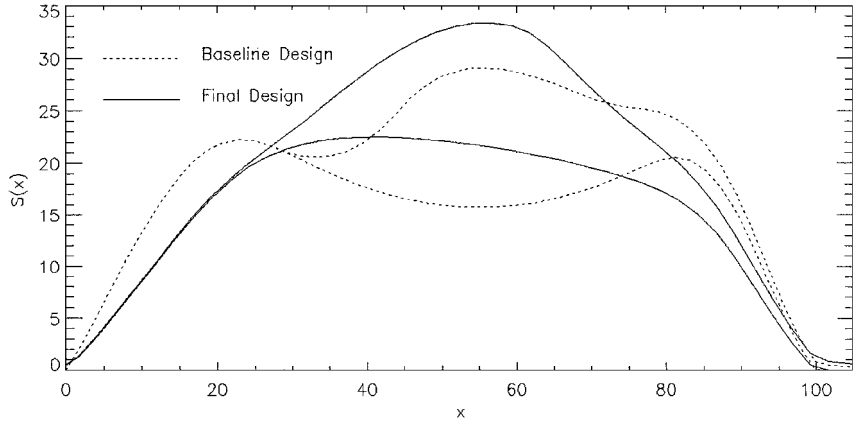

d) ($p_1 = 0.0; p_2 = 1.0$) design problem

Fig. 5 Average area distributions of the equivalent bodies of revolution of the baseline and HSCT designs.

problems, and the most optimal designs obtained were selected for presentation. Tables 2a and 2b give the final parameter values and the final coefficients of lift and wave drag of the best final HSCT designs obtained for each of the four design problems.

These tables show that, as the values of the weighting parameters p_1 and p_2 vary from the subsonic end of the design spectrum to the supersonic end, both the final values of lift and wave drag decrease. The percentage improvements, with respect to the initial HSCT, in all of the design problems considered were substantial. For example, in the subsonic case a 42.58% increase in the lift was achieved (with a 49.53% increase in wave drag), whereas in the supersonic case (Mach 2) a 56.18% reduction in wave drag was achieved (with a 38.89% reduction in lift).

Figures 3a–3d illustrate the final HSCT configurations of the four design problems. The principal design variations as the influence of the supersonic design criterion increases are an increase in the wing sweep, a decrease in the chord length c_2 of the wing crank, an increase in the spanwise position y_{w_2} of the wing crank, and a decrease in the waisting of the fuselage. The HSCT configurations of Figs. 3b and 3c, which correspond to the two multipoint design problems, bear the most resemblance to existing supersonic aircraft, and this indicates that a consideration of multiple design points will yield more plausible aircraft designs.

Figures 4a–4d illustrate the spanwise variations of the section coefficients of lift of the four final HSCT designs and, also, of the baseline HSCT. These figures show clearly that the section coefficients of lift are reduced as the influence of the supersonic design criterion is increased. Figures 5a–5d illustrate the average cross-sectional area distributions of the equivalent bodies of revolution (evaluated as part of the supersonic wave drag analysis) of each of these HSCT designs. These figures show that, as the influence of the supersonic design criterion increases, the average cross-sectional area distributions of the equivalent bodies of revolution become smoother and more symmetrical. Because a technique for wave-drag reduction, sometimes referred to as *coke-bottling*, results in a waisted fuselage, it is surprising that the waisting of the fuselages in Figs. 5a–5d reduces as the influence of the supersonic criterion is increased. However, the average cross-sectional area distribution of the supersonic single point design problem is very similar to the desired bell-shaped distribution of the already mentioned Sears–Haack body.

A problem encountered in optimizing the supersonic wave drag obtained from the Harris program was a rather haphazard convergence. (A similar problem was also reported by Hutchison et al.[25] in the optimization of a HSCT using wave-drag data obtained from the Harris program.) It appears, in this work, that this problem arose because of the presence of many minima in the wave drag, which have very narrow and steep-sided basins of attraction. Although small step lengths were imposed upon the line searches in the optimization process, the optimizer was able to jump from one minimum to another. Previous work[26] in this area has considered the use of simulated annealing—a global method of optimization. However, this method performs well when a global minimum is surrounded by much poorer minima and is therefore not suited to this problem where the abundance of similar minima inhibit the location of the global minimum.

Conclusions

An application of the PDE method to the generation and subsequent multipoint design of an HSCT has been illustrated. Allowing only 21 design parameters to vary, substantial reductions in the multipoint design criteria of the HSCT were obtained. The wide diversity of the aircraft geometries exhibited by the baseline and final HSCT designs illustrate not only the effect of varying the influence of different design points in the optimization process but also the capability of the PDE method to succinctly parameterize complex geometries while still maintaining sufficient flexibility in the range of possible shapes.

Acknowledgment

The authors would like to thank the Engineering and Physical Sciences Research Council (EPSRC) for financial support (Research Grant GR/L11366).

References

[1]Wilhite, A. W., and Shaw, R. J., "HSCT Research Picks up Speed," *Aerospace America*, Vol. 35, No. 8, Aug. 1997, pp. 25–29, 41.

[2]Ashley, H., *Engineering Analysis of Flight Vehicles*, Dover, New York, 1974, pp. 4, 5.

[3]Thibert, J. J., "One Point and Multipoint Design Optimization for Aircraft and Helicopter Application," *Special Course on Inverse Methods for Airfoil Design for Aeronautical and Turbomachinery Applications*, AGARD-R-780, May 1990, pp. 10.1–10.47.

[4]Labrujère, Th. E., and Slooff, J. W., "Computational Methods for the Aerodynamic Design of Aircraft Components," *Annual Review of Fluid Mechanics*, Vol. 25, 1993, pp. 183–214.

[5]Bloor, M. I. G., and Wilson, M. J., "Generating Blend Surfaces Using Partial Differential Equations," *Computer-Aided Design*, Vol. 21, No. 3, 1989, pp. 165–171.

[6]Bloor, M. I. G., and Wilson, M. J., "Using Partial Differential Equations to Generate Free-Form Surfaces," *Computer-Aided Design*, Vol. 22, No. 4, 1990, pp. 202–212.

[7]Bloor, M. I. G., and Wilson, M. J., "Efficient Parametrization of Generic Aircraft Geometry," *Journal of Aircraft*, Vol. 32, No. 6, 1995, pp. 1269–1275.

[8]Smith, R. E., Bloor, M. I. G., Wilson, M. J., and Thomas, A. M., "Rapid Airplane Parametric Input Design (RAPID)," AIAA Paper 95-1687, June 1995.

[9]Dekanski, C. W., Bloor, M. I. G., and Wilson, M. J., "The Generation of Propeller Blade Geometries Using the PDE Method," *Journal of Ship Research*, Vol. 39, No. 2, 1995, pp. 108–116.

[10]Sevant, N. E., Bloor, M. I. G., and Wilson, M. J., "Aerodynamic Design of a Wing-Body Combination," *Creating Fair and Shape-Preserving Curves and Surfaces*, edited by H. Nowacki and P. D. Kaklis, B. G. Teubner Stuttgart, Leipzig, Germany, 1998, pp. 271–280.

[11]Bloor, M. I. G., and Wilson, M. J., "Spectral Approximations to PDE Surfaces," *Computer-Aided Design*, Vol. 28, No. 2, 1996, pp. 145–152.

[12]Ashby, D. L., Dudley, M. R., Iguchi, S. K., Browne, L., and Katz, J., "Potential Flow Theory and Operation Guide for the Panel Code PMARC," NASA-TM-102851, Jan. 1991.

[13]Ashley, H., and Landahl, M., *Aerodynamics of Wings and Bodies*, Dover, New York, 1985, pp. 173–191.

[14]Harris, R. V., Jr., "An Analysis and Correlation of Aircraft Wave Drag," NASA TM X-947, March 1964.

[15]von Kármán, Th., *The Problem of Resistance in Compressible Fluids*, Atti del V Convegno della Fondazione Alessandro Volta, Rome, 1935, pp. 222–276.

[16]Jones, R. T., "Theory of Wing-Body Drag at Supersonic Speeds," NACA Rept. 1284 (Supersedes NACA RM A53H18a, 1953), 1956.

[17]Whitcomb, R. T., and Sevier, J. R., Jr., "A Supersonic Area Rule and an Application to the Design of a Wing-Body Combination with High Lift-Drag Ratios," NASA TR R-72 (Supersedes NACA RM L53H31a, 1953), 1960.

[18]Hayes, W. D., "Linearized Supersonic Flow," North American Aviation, Rept. A.L. 222, Los Angeles, June 1947.

[19]Raymer, D. P., *Aircraft Design: A Conceptual Approach*, AIAA Education Series, AIAA, Washington, DC, 1992, p. 262.

[20]Sears, W., "On Projectiles of Minimum Wave Drag," *Quarterly of Applied Mathematics*, Vol. 4, No. 4, 1947, pp. 361–366.

[21]Haack, W., *Geschussformen kleinsten Wellenwiederstandes*, Bericht 139, Lilienthal–Gesellschaft, 1947.

[22]Press, W. H., Teukolsky, S. A., Vetterling, W. T., and Flannery, B. P., *Numerical Recipes in FORTRAN*, Cambridge Univ. Press, Cambridge, England, U.K., 1992, pp. 418–423.

[23]Bischof, C., Carle, A., Khademi, P., and Mauer, A., "ADIFOR 2.0: Automatic Differentiation of Fortran 77 Programs," *IEEE Computational Science and Engineering*, Vol. 3, No. 3, 1996, pp. 18–32.

[24]Fletcher, R., *Practical Methods of Optimization*, Wiley, New York, 1987, pp. 240–245.

[25]Hutchison, M., Unger, E., Mason, W., Grossman, B., and Haftka, R., "Variable-Complexity Aerodynamic Optimization of an HSCT Wing Using Structural Wing-Weight Equations," AIAA Paper 92-0212, Jan. 1992.

[26]Sevant, N. E., "Automated Optimal Aerodynamic Design," Ph.D. Dissertation, Dept. of Applied Mathematical Studies, Univ. of Leeds, England, UK, Sept. 1997.